The Search for Optimum Configurations for Re-entry Vehicles

Tony C. Lin*and Wallis R. Grabowsky†
TRW Electronics and Defense Sector, San Bernardino, California
and
Kevin E. Yelmgren‡
Ballistic Missile Office, Norton AFB, San Bernardino, California

This paper describes an investigation to identify possible optimum re-entry vehicle configurations. The criteria for selecting the optimum re-entry vehicle shapes are based on aerodynamic stability, nosetip/frustum boundary-layer transition onset and propagation, asymmetric nosetip shape change induced trim, minimization of re-entry dispersion, and booster sizing/weight limitation. The numerical results indicate that a highly oblate nose shape (e.g., a flat-faced nose or 5×1 ellipse) has a better performance potential when compared to a spherical nose using the above criteria. For the aft body, only biconic shapes are considered and the optimum bicone is believed to have the following characteristics: $\theta_1 \approx 2\theta_2$ and $R_b \approx 2R_J$ where θ_1, θ_2 are the fore and aft cone angles, respectively, R_J the local radius at bicone juncture, and R_b the re-entry vehicle base radius. Under these restrictions, improvement in re-entry vehicle aerothermodynamic performance, e.g., small $X_{c.p.}$ variation with M_∞ and α; minimum ablated nosetip downstream influence may be achieved with possibly no degradation in frustum boundary-layer transition performance. Consideration also is given to the disadvantages of using these suggested optimum re-entry vehicle configurations.

Nomenclature

A	= re-entry vehicle base area
C_A	= axial force coefficient
C_D	= drag coefficient
C_{m_α}, C_{n_β}	= pitch and yaw static stability derivative
D	= re-entry vehicle drag
L	= re-entry vehicle lift force; vehicle axial length measured from the nose stagnation point
L_v	= vehicle axial length measured from the virtual apex
M_∞	= freestream Mach number
p	= pressure
p_{t2}	= Rayleigh pitot pressure
R_N	= re-entry vehicle nose radius
R_b	= re-entry vehicle base radius
Re	= Reynolds number
R_J	= local radius at bicone juncture
R_f	= flat-face radius
r_c	= flat-face corner radius
s	= distance measured from the stagnation point
U_e	= boundary-layer edge velocity
U_∞	= freestream velocity
W	= re-entry vehicle weight
$X_{c.p.}$	= location of the center of pressure
α	= angle of attack
β	= ballistic coefficient, $= W/C_D A$
γ	= ratio of specific heat
Δ	= shock standoff distance
$\theta 1$, $\theta 2$	= re-entry vehicle conic angle (see Fig. 1)
θ_N	= nose bicone angle (see Fig. 1)

Submitted Feb. 4, 1983; revision received July 18, 1983.

*Section Head. Member AIAA.
†Department Head, Aeromechanics and Propulsion. Member AIAA.
‡Major, USAF. Member AIAA.

Introduction

AFTER nearly 40 years of missile development, the typical re-entry vehicle (RV) configuration still consists of a spherical nose with a simple conical afterbody. The majority of early optimization studies were devoted to the determination of minimum drag bodies.[1] Recently, more work has appeared that minimizes the heat transfer to the nosetip of the vehicle.[2-7] The initial limitation of constant freestream conditions[2-4] was removed by Baker and Kramer.[5,6] Their approach, which used the calculus of variations, minimized the total heat transfer to a nosetip on a constant β trajectory. Yelmgren[7] removed this limitation using the variation of parameters method. All of these studies concluded that the flat face was the optimum shape for minimizing the heat loading to the nosetip.

The aft body has not received as much attention as the nosetip. From a heat-transfer point of view, the aft body is less critical than the nosetip. However, from an overall systems performance point of view, the aft body does become important. Specifically, considering aerodynamic stability, boundary-layer transition (BLT) onset and propagation, and warhead packaging, the aft body plays a major role. In general, the biconic or triconic body has been assumed to be the optimum aft body§ and, consequently, it is the only general configuration addressed in this paper. None of the previous studies have attempted to optimize the total re-entry vehicle from an overall systems standpoint. A possible optimum re-entry vehicle will be developed here with the major disadvantages also being identified.

It must be noted that the RV materials, as well as the RV configuration, can improve RV performance. Extensive analytical investigation and ground testing has been carried out to select the optimum nosetip and frustum materials. For example, nosetip material tradeoff studies have been made among high-altitude transitional rough materials (HAT), low-altitude transitional smooth materials (LAT), shape-stable composite nose material (SSN), and erosion-resistant nose material (ERNM). Some of these material concepts and their derivatives have been flight tested as well as ground tested

§The ogive configuration is not considered here since in most cases it would render less favorable RV stability.

with varied results, as reported in Refs. 8-10. Further discussion on this subject is beyond the scope of the present paper.

As can be imagined, it is difficult to determine a universally optimum RV configuration since it is influenced by many factors. Principal among these is the mission for the RV. For example, for terminal evasion requiring a maneuvering RV, a sharp nosetip is perferred because a high L/D is essential for its performance. For ballistic flight, a blunt nosetip may be desirable when considering nosetip/frustum heating. After the RV mission, thermal protection materials requirements, aerodynamic stability, ballistic coefficient, warhead sizes and shapes, as well as space available under the missile shroud, are major factors to be considered in selecting the RV geometry and materials. Here we shall address the issues of RV thermal protection, aerodynamic stability (static margin), RV nose shape change (minimize re-entry dispersion and nosetip loads), and booster sizing/weight limitations. The nosetip/frustum shapes which will be considered are illustrated in Fig. 1. Assessment and comparison of these configurations will be made against a sphere-cone configuration.

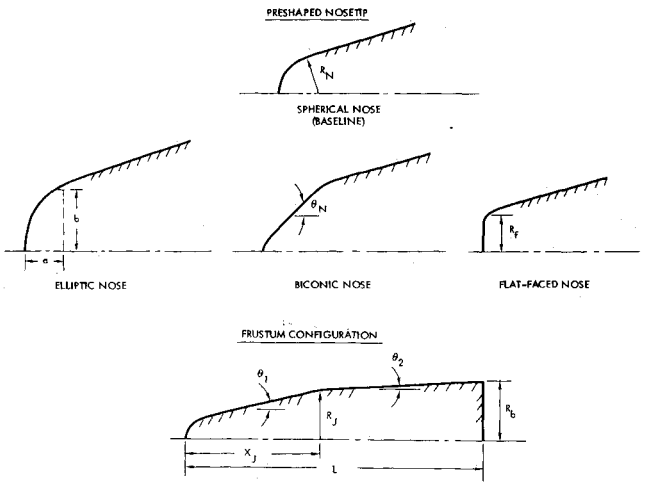

Fig. 1 Preshaped nosetip and biconic aft configuration.

Nosetip

Thermal Protection

Thermal protection of the RV is essential for survival during re-entry. Thermal protection requirements can be reduced by minimizing the total heat input to the vehicle along the re-entry trajectory. Baker and Kramer[5,6] determined that a truncated conic with a flat-face nose is an optimum shape and its flat-face diameter decreased as the fineness ratio decreased. They found that the heat transfer can be reduced by 30% of that of a spherical nose. More recent calculations made for a transpiration cooled nosetip design are given in Table 1.[11] As indicated, the total coolant flow rate required on a flat face with a small corner radius is significantly lower than on a spherical nose (0.024 vs 0.0644 kg/s).

Clear air nosetip shape change calculations were performed in order to investigate the effect of using a flat-faced nose instead of a spherical one. Numerical results, using TRW-SCATHE,[12] are given in Figs. 2 and 3 for a spherical nose and flat-face nose, respectively. Herein the criterion for determining the boundary-layer transition is the same for both nose shapes and the following correlation is used[12]:

$$Re_\theta = 544\left[\frac{k}{\theta}\frac{T_e}{T_w}\right]^{-1.55}$$

where k is the nose material intrinsic roughness, θ the momentum thickness, $Re = \rho_e U_e \theta/\mu_e$, and T_e/T_w the temperature ratio between boundary-layer edge and wall.

The calculated results correspond to $R_N = 0.0889$ m (3.5 in.) and $\beta = 9765$ kg/m^2 (2000 psf) and show that the flat-face nosetip recedes much less than the spherical nosetip (1.397 vs 6.43 cm). Obviously, the difference in the total recession between a flat-face nosetip and a spherical nosetip is much greater than 30%, as suggested by Baker and Kramer.[5] One cause is the slower propagation of boundary-layer transition over the front of the flat-face nose.

Nosetip Boundary-Layer Transition and Shape Change

As turbulent heat transfer is usually higher than laminar heating, any nose configuration (or material) that can delay transition during re-entry is preferred, assuming all other factors remain the same. In addition to selecting a smooth material, another approach is to control the nosetip local Reynolds number and pressure gradient. This can be achieved

Table 1 Shape optimization study for total ideal coolant required[a] (TCNT)

CANDIDATE NOSE SHAPE	HEMISPHERICAL	LARGE SPHERICAL RADIUS	FLAT FACE 0.13 & 0.38 cm RADIUS CORNER		FLAT STAGNATION POINT SMALL RADIUS CORNER
CONFIGURATION	1 1.65 cm R_N SPHERE	2 3.43 cm R_N SPHERE	3 FLAT FACE .127 cm R_C	4 FLAT FACE 0.38 cm R_C	5 FLAT FACE 75° CONE
BASE DIAMETER, cm	3.15	3.15	3.15	3.15	3.15
TOTAL COOLED AREA, cm^2	11.87	8.26	11.03	9.87	8.06
MAXIMUM IDEAL FLOW RATE*, gm/sec	64.4	54.4	24.0	39.	62.6
MAXIMUM IDEAL MASS FLUX*, gm/cm^2 - sec	9.765	8.3	16.6	15.62	9.765
LOCATION OF MAXIMUM $\dot{m}$ OR $\dot{q}$, S, cm	0.762	1.524	1.524	1.321	1.524

CONCLUSION: • FLAT FACE SMALL CORNER RADIUS REQUIRES LEAST TOTAL COOLANT
• FLAT FACE SMALL CORNER RADIUS REQUIRES HIGHEST LOCAL MASS FLUX (AT CORNER)

[a] For AEDC-track G conditions: $V_\infty = 5181.6$ m/sec, $P_\infty = 350$ Torr, LWC = 1.0 g/m^3

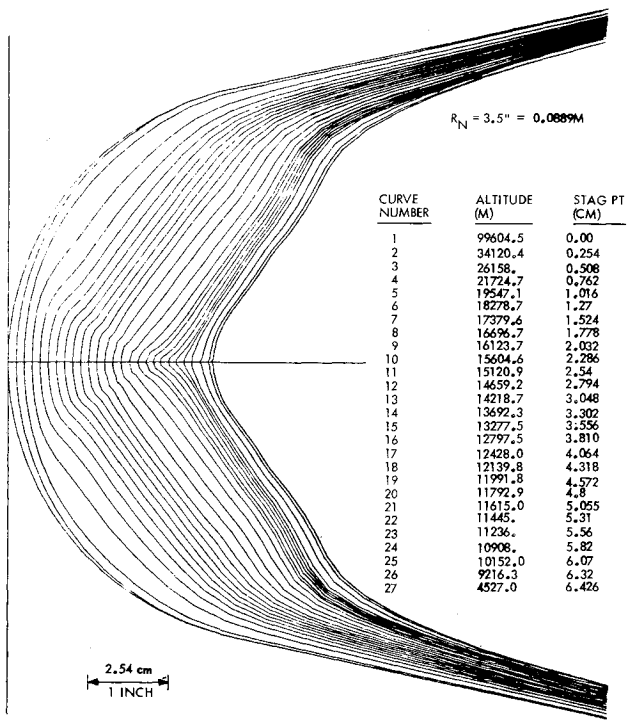

CURVE NUMBER	ALTITUDE (M)	STAG PT (CM)
1	99604.5	0.00
2	34120.4	0.254
3	26158.	0.508
4	21724.7	0.762
5	19547.1	1.016
6	18278.7	1.27
7	17379.6	1.524
8	16696.7	1.778
9	16123.7	2.032
10	15604.6	2.286
11	15120.9	2.54
12	14659.2	2.794
13	14218.7	3.048
14	13692.3	3.302
15	13277.5	3.556
16	12797.5	3.810
17	12428.0	4.064
18	12139.8	4.318
19	11991.8	4.572
20	11792.9	4.8
21	11615.0	5.055
22	11445.	5.31
23	11236.	5.56
24	10908.	5.82
25	10152.0	6.07
26	9216.3	6.32
27	4527.0	6.426

Fig. 2 Numerical results[12] of spherical nosetip shape change history.

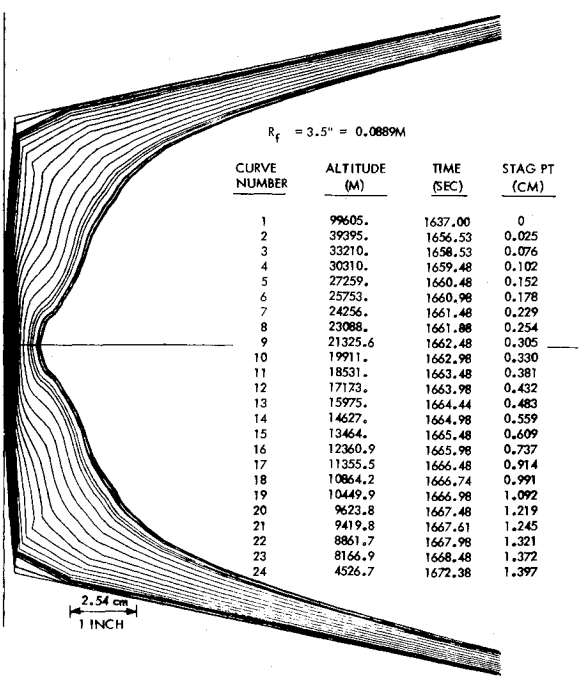

CURVE NUMBER	ALTITUDE (M)	TIME (SEC)	STAG PT (CM)
1	99605.	1637.00	0
2	39395.	1656.53	0.025
3	33210.	1658.53	0.076
4	30310.	1659.48	0.102
5	27259.	1660.48	0.152
6	25753.	1660.98	0.178
7	24256.	1661.48	0.229
8	23088.	1661.88	0.254
9	21325.6	1662.48	0.305
10	19911.	1662.98	0.330
11	18531.	1663.48	0.381
12	17173.	1663.98	0.432
13	15975.	1664.44	0.483
14	14627.	1664.98	0.559
15	13464.	1665.48	0.609
16	12360.9	1665.98	0.737
17	11355.5	1666.48	0.914
18	10864.2	1666.74	0.991
19	10449.9	1666.98	1.092
20	9623.8	1667.48	1.219
21	9419.8	1667.61	1.245
22	8861.7	1667.98	1.321
23	8166.9	1668.48	1.372
24	4526.7	1672.38	1.397

Fig. 3 Numerical results[12] of nose shape change history for a preshaped nose (truncated cone).

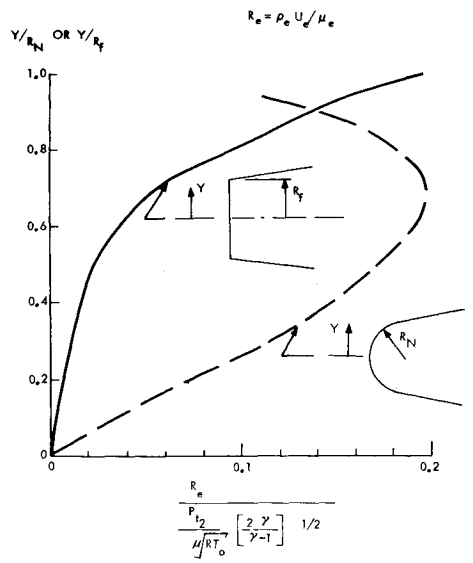

Fig. 4 Local Reynolds number vs Y for preshaped nosetip and spherical nose.

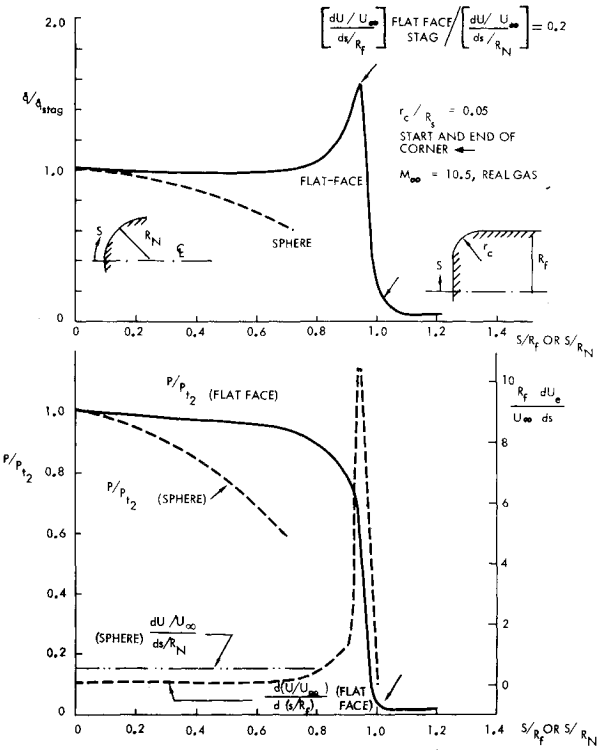

Fig. 5 Heating rate and velocity gradient on a flat-face nosetip.[24]

with an oblate-shaped nosetip. A comparison of local Reynolds number vs distance along a flat-face cone and a sphere cone is shown in Fig. 4. As can be seen, the flat-faced body has the lower unit Reynolds number, Re. This would result in a slower transition front propagation on the flat-faced nosetip. The numerical results for the shape change occurring with the spherical nose, Fig. 2, indicate that sonic point ($y/R_N \sim 0.70$) transition occurs at about 28.96 km (95 kft). This corresponds to a material intrinsic roughness of 1.8 mil when PANT transition criteria[13] are employed. For the same roughness height, the flat-faced nosetip sonic point (i.e., the shoulder) transition also occurred at approximately 28.96 km, but the transition front did not reach $y/R_f \sim 0.70$ until 20.42 km (see Fig. 3). At this altitude (i.e., $h = 20.42$ km), the spherical nose already had evolved into mildly indented nose shape and the stagnation-point had 0.889 cm recession (see Fig. 2); while the ablate nose only had 0.3048 cm stagnation-point ablation (Fig. 3).

A comparison of Figs. 2 and 3 shows that nosetip shape change occurs more slowly on the flat-face nosetip. This is due to a lower value of stagnation-point velocity gradient, du/dx (Fig. 5), and a slower nosetip transition front propagation occurring on an oblate nosetip. This would

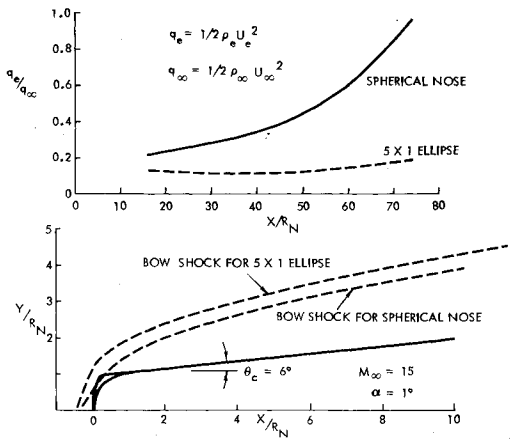

Fig. 6 Numerical results of shock envelopes and boundary-layer dynamic pressure for two nosetips.

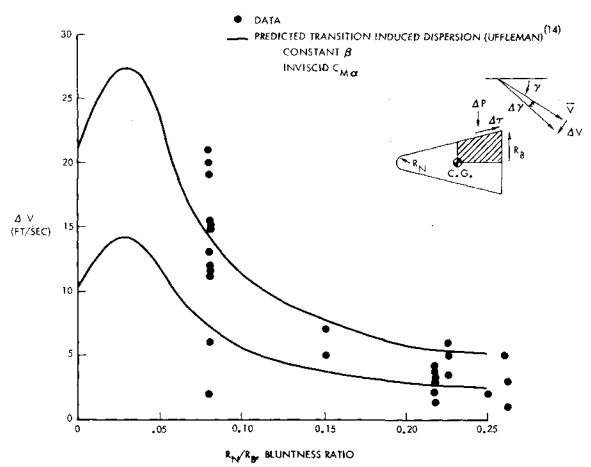

Fig. 7 BLT induced ΔV vs bluntness ratio.

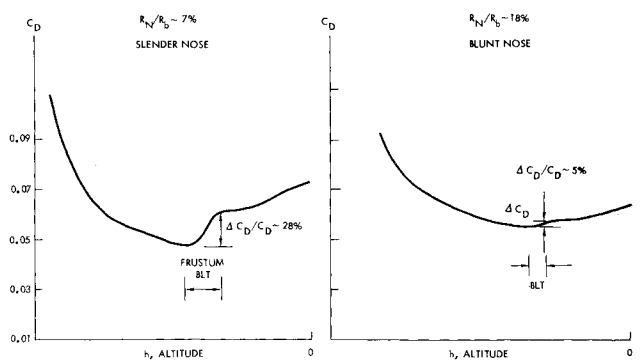

Fig. 8 Schematics illustrating the drag perturbation at frustum BLT altitude.

reduce the probability of nosetip ablation. This translates into smaller drag-induced range errors and reduced nosetip overhang requirements.

Downstream Influences

It is known that a slender RV with a blunt nose creates a thick entropy layer with steep gradients. The values of the boundary-layer edge properties are influenced strongly by the entropy gradients. Consequently, the frustum heating and shear stresses also are affected by this phenomena. Comparisons of shock shapes and boundary-layer edge dynamic

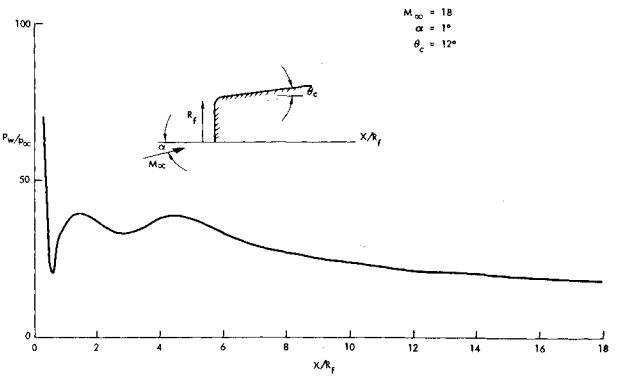

Fig. 9 Numerical results of windward plane surface pressure distribution on a flat-faced conical body.[26,27]

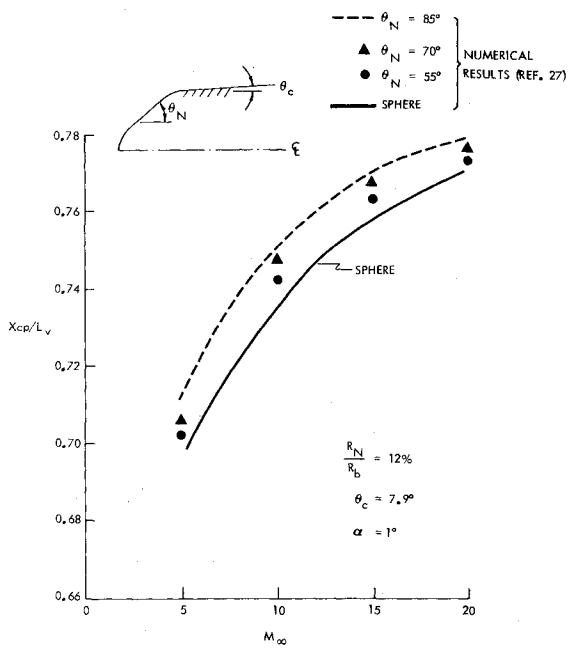

Fig. 10 Numerical results of $X_{c.p.}/L$ vs M_∞ for preshaped nosetip.[27]

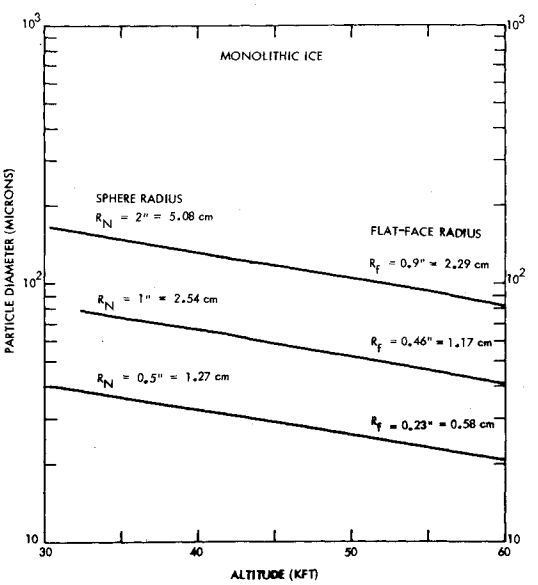

Fig. 11 Minimum-size particle surviving the stagnation region shock layer.[18]

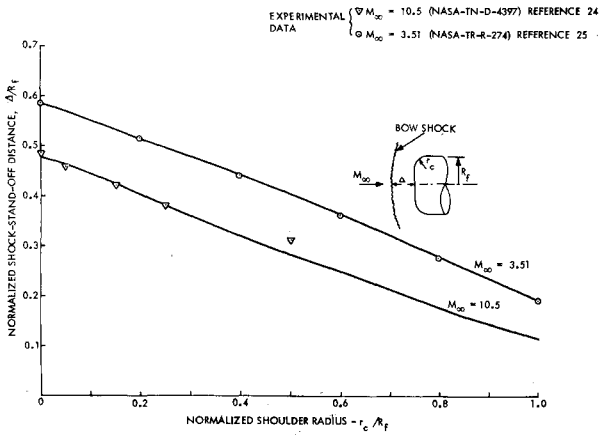

Fig. 12 Blunt-body shock standoff distance correlation.

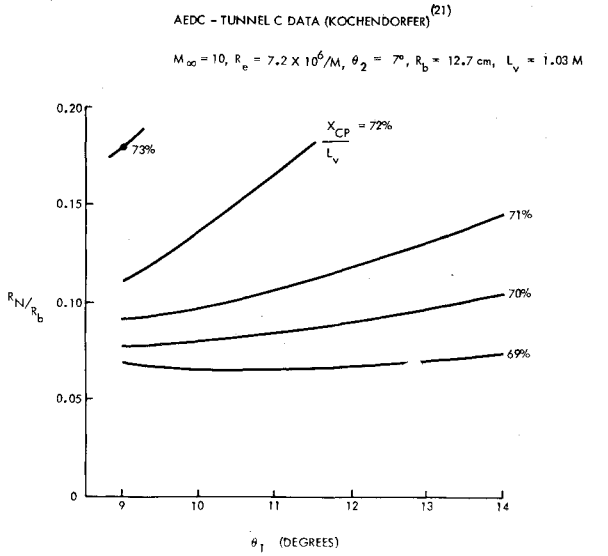

Fig. 13a Experimental measurements of center of pressure contours for $R_J/R_b = 45\%$.

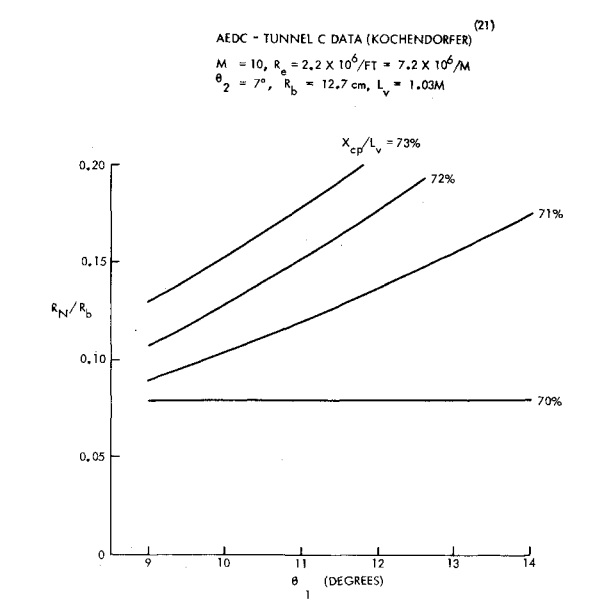

Fig. 13b Experimental measurements of center of pressure contours for $R_J/R_b = 60\%$.

pressure are shown in Fig. 6 for a spherical nose and a 5×1 elliptical nose. The spherical radius R_N and the elliptical shoulder height are assumed to be the same value. Clearly the frustum dynamic pressure on the elliptical nose is much smaller than on the spherical nose. This is due to differences in the nosetip shock shape and the effects of entropy layer swallowing. Consequently one would expect that the frustum heat transfer would be lower for the elliptical nose, and any RV dispersion due to asymmetrical BLT also would be smaller for the elliptical nose cone configuration (see Fig. 7).[14]

The viscous shear stress (C_f) can contribute from 20 to 40% of the total drag (C_D) on a slender RV. However, the C_f contribution to C_D can be as low as 5% on a blunt RV. Therefore, the effects of BLT upon the vehicle drag perturbation are much less on the blunt RV, e.g., flat-faced nosetip, than on a slender RV, Fig. 8. Generally, the RV designers are required to maintain β or C_D within a prescribed narrow band. Under this restriction one can reduce the oblate nosetip shoulder radius (e.g., $R_f = R_N/1.35$) in order to meet the β requirement.

The surface pressure distribution downstream of a flat-faced nose with a conical aft body is shown in Fig. 9. Note that a recompression region exists right after the overexpansion at the flat-face corner. This adverse pressure gradient may serve to promote frustum boundary-layer transition,[5,15] which may cause rapid uniform movement of the frustum transition front to the nosetip and thereby reduce asymmetry BLT perturbations. This would help in reducing the trajectory disperison.

Effects of Nose Shape on Aerodynamic Stability

As mentioned previously, there are potential benefits for improving aerodynamic stability, e.g., the static margin, by using a preshaped nosetip. Crose et al.[16] optimized the initial nosetip shape with consideration of re-entry shape change and to minimize RV dispersions. Their results indicated a 48 deg biconic nose would yield the minimum CEP for the class of vehicles they studied. Hall et al.[17] made a sophisticated study with numerical finite difference codes to estimate the effects of a preshaped nose and the nose shape change on aerodynamic stability. They concluded that a 55 deg biconic nose offered a significant advantage in static margin increase and shape stability relative to an initially spherical nose.

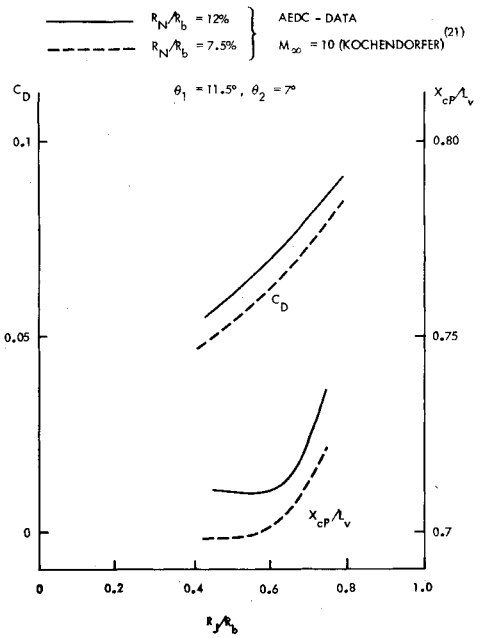

Fig. 14 $X_{c.p.}/L_v$ and C_D distributions—experimental results.

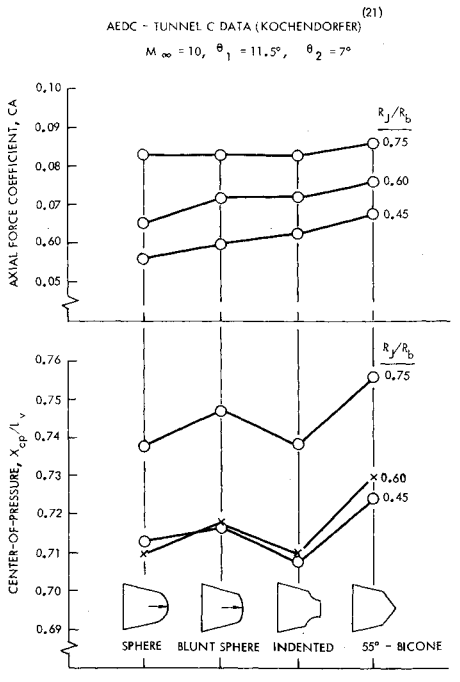

Fig. 15 Nonspherically blunted nosetip axial force coefficient and center of pressure experimental measurements.[21]

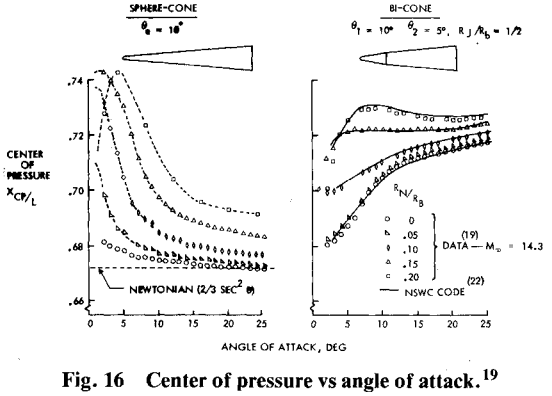

Fig. 16 Center of pressure vs angle of attack.[19]

Figure 10 depicts the location of pitch center of pressure for several nose shapes. The baseline (spherical nose) solutions would have the most forward center of pressure locations while bicone noses with $\theta_N = 55$, 70, and 85 deg would shift $X_{c.p.}$ progressively aftward. For this specific case, the biggest static margin is obtained with the largest value of biconic nose angle (i.e., $\theta_N = 85$ deg). Thus the inviscid flow numerical results demonstrate that a preshaped nose (particularly, $\theta_N \rightarrow 90$ deg, potentially can increase the static margin of the RV.

Weather

Re-entry through weather also is a factor that must be considered when designing future RVs. The amount of thermal (e.g., nosetip overhang) protection required will be determined by weather requirements. The recession rate of passive nosetips in weather depends directly on the mass of the ice or rain that survives the shock layer and impacts the vehicle nosetip. The thicker the shock layer, the less mass hits the nosetip because the shock layer would decelerate the ambient particulates. At the same time the high dynamic pressure and hot environment would melt, evaporate, and even break up the ice crystals or rain drops when they traverse across the shock layer.[18] This is illustrated in Fig. 11, which shows the minimum diameter of ice particles that could

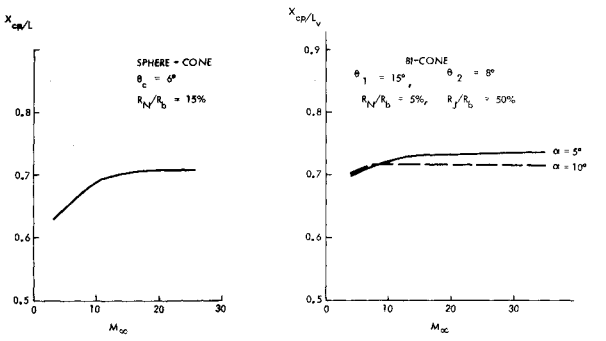

Fig. 17 Numerical results for $X_{c.p.}/L$ vs M_∞ for bicone and simple conic body.[27]

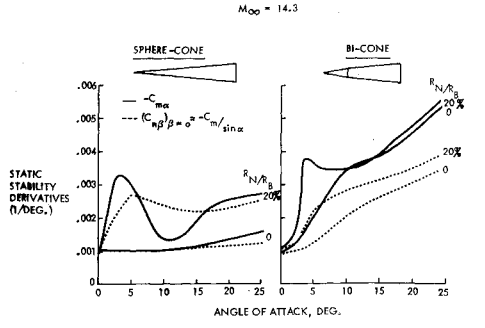

Fig. 18 C_{m_α} and C_{n_β} vs angle of attack[21] experimental measurement with moment center at $0.65L$.

survive the shock layer and strike the nosetip without breaking up or melting away. For example, at 12.19 km, a 2.54-cm spherical nosetip would experience weather erosion from freestream ice particles greater than 65 μ diameter. However, the shock layer of a flat-face nosetip is almost three times that of the hemisphere (Fig. 12) and correspondingly experiences erosion only from ice particles greater than 140 μ diameter. Hence the flat-face nose has an advantage over the hemisphere from an erosion standpoint since it reduces the magnitude of the weather environment effectively by eliminating the impacting mass of the smaller particle.

The current state-of-the-art in nose shape change prediction in a highly erosive environment (LWC ≥ 0.2 g/m^3) results in a flat face, regardless of the original nose shape. Therefore, using a flat or oblate nose shape at re-entry would result in minimum shape variations through weather. This again would imply minimum drag variation induced range error.

The Aft Body

The outer configuration of the RV is influenced by RV ballistic coefficient requirements, booster shroud, and the payload restriction. Usually a tradeoff between ballistic coefficient, nosetip overhang, RV weight, and RV aerodynamic stability constrained by payload shape, base diameter, and booster shroud contour will determine the RV frustum cone angles. The usage of a multiconical body gives an additional degree of flexibility for optimizing designs. For instance, it gives a flexible means to accommodate the nosetip overhang and booster sizing/payload packaging issues. However, it is important to realize that certain combinations of θ_1, θ_2, and R_J/R_b (see Fig. 1) can result in improved aerodynamic performance.

Aerodynamics

Extensive wind tunnel measurements for bicone aerodynamics were conducted by Stetson et al.,[19] Chaussee et

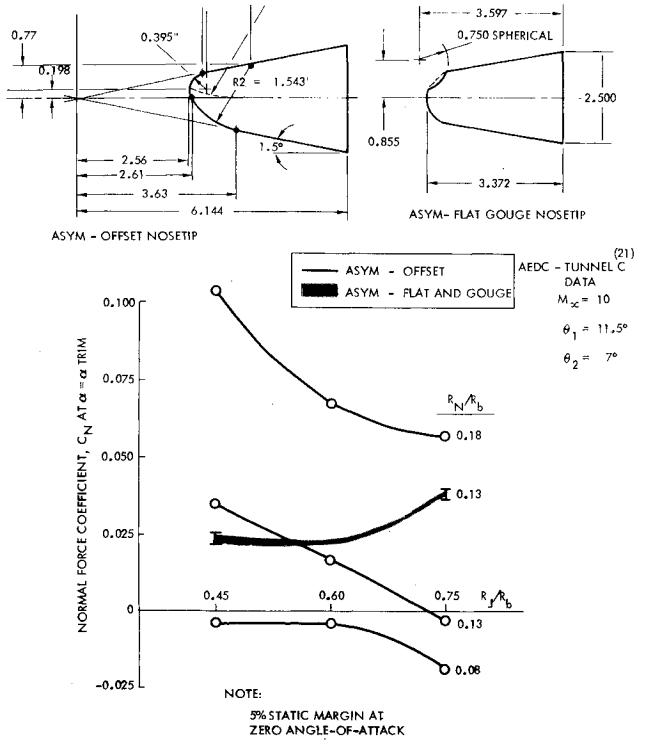

Fig. 19 Trimmed normal force coefficient vs biconic joint location.[21]

al.,[20] and Kochendorfer[21] to determine the aero performance as a function of the nose ablation and the vehicle geometric parameters, e.g., θ_1, θ_2, R_J/R_b, and R_N/R_b. Figures 13 and 14 depict the center of pressure contour for a bicone whose aft cone angle, θ_2, is 7 deg. Note that $X_{c.p.}/L$ moves aftward when one increases R_J/R_b or θ_1. However, the drag also increases significantly as R_J/R_b increases (Figs. 14 and 15). This large increase in C_A can become unacceptable to RV designers. Moreover, as R_J/R_b increase, the RV becomes shorter to the point that the payload will not package. Also, it is noted that the $X_{c.p.}/L$ movement is not sensitive to biconic juncture position when $0.4 < R_J/R_b < 0.6$ (see Fig. 14). This type of stability distribution would render designers flexibility in locating the RV center of gravity, payload compartment, and nosetip overhangs. Based on these experimental results, many numerical inviscid flow computations, payload packaging requirements, and minimum drag considerations, it is suggested that bicones with $\theta_1 \approx 2\theta_2$ and $R_b \approx 2R_J$ may be candidates for optimum RV configurations. This recommendation is further reinforced by Stetson and Lewis' data,[19] whose test model configurations happen to comply with the suggested geometry criterion. Figure 16 shows the measured, as well as calculated, center of pressure location vs angle of attack α at $M_\infty = 14.3$ for a cone and bicone. The calculated $X_{c.p.}/L$ vs freestream Mach number M_∞ is illustrated in Fig. 17. These results indicate the biconic configuration reduces the effect of nosetip bluntness, has a smaller center of pressure movement with α and M_∞, and has a greater static stability at large angle of attack when compared with the sphere-cone configuration.

It should be noted that the static stability derivatives, C_{m_α}, for the bicone are nonlinear with angle of attack and that the in-plane and out-of-plane derivatives (i.e., C_{m_α} and C_{n_β}) are not equal. With the exception of a sharp cone, the sphere-cone has similar trends (see Fig. 18), hence, in this regard, there is no payoff for using a bicone configuration.

Frustum Boundary-Layer Transition

References 22 and 23 have made experimental measurements for investigating frustum boundary-layer transition on

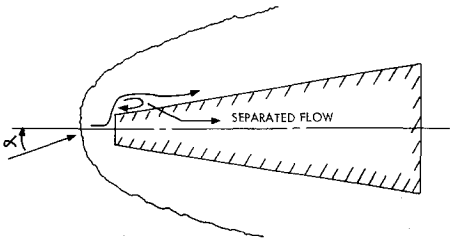

Fig. 20 A schematic of leeward plane flow separation.

simple conic shapes and bicones. They independently found that, for practical configurations of interest, the biconic joint has no perceptible influence on frustum transiton, which suggests that there is no degradation of BLT performance when a biconic RV is employed.

Ablated-Nose Downstream Influence

One undesirable result of nosetip asymmetry for current ballistic RV design is the dispersion caused by nonaverage vehicle lateral or lift force and, consequently, smaller trimmed normal forces are preferred. Figure 19 shows the wind tunnel measured normal force coefficient at trim angle of attack which is caused by an ablation-induced asymmetric nosetip. For this comparison the trim angles of attack were computed assuming a static margin of 5% of the vehicle length at zero angle of attack. It is noted that the magnitude/variation of C_N with biconic joint location (i.e., R_J/R_b) appears to depend on the type of asymmetry. However, a proper selection of R_J/R_b (e.g., 50%) may alleviate the effects of nosetip ablation-induced loads and RV dispersion.

Additional Considerations

The advantages of using an oblate nosetip and biconic frustum configurations have been discussed; however, there is still some concern about using these configurations which are listed below.

1) Most of the advantages of using a flat-face or oblate elliptic nose are deduced from analytic calculations. Experimental results (both wind tunnel measurements and flight test) are needed to confirm the validity of numerical results. For instance, there is concern about the viscous effects at the shoulder of the flat-face nose where local flow separations may occur, particularly in laminar flow (Fig. 20).

2) Geometries involving shape curvature discontinuities may cause adverse effects upon local surface ablation. Additionally, geometrical effects upon radar cross section (RCS) and radar frequency (RF) performance require investigation since surface geometry changes also will change characteristic plasma effect, i.e., it is expected that a flat-face nose will result in a higher sheathing altitude than a spherical nose.¶

3) The flat-face nose would require a smaller amount of nose coolant when a transpiration cooled nosetip (TCNT) active system is used; however, it also requires larger local blowing rates at the nose corner. (See Table 1.)

4) The effects of a preshaped nose as well as multiconic frustums upon RV roll dynamics are unknown. Ground simulations and flight tests are needed to resolve ths issue.

5) The sonic point on the flat-face nosetip is located at the shoulder where the nosetip boundary-layer transitions would first occur during re-entry. In the event that the nosetip asymmetric transition patterns arise, then they would appear at the location of a larger radius (i.e., larger area) as compared to that on a spherical nose. Consequently, the resulting trim angle may become larger on the flat-face nose. Ex-

¶This is referred to the case when $R_f = R_N$, Fig. 1.

perimental measurements are required to verify this reasoning. Also, ground tests are needed to consider the effects of a large favorable pressure gradient upon the nosetip boundary-layer transition.

Summary

An investigation has been made from the existing literature to determine the optimum nose shape and aft frustum configuration in an effort to improve re-entry vehicle performance. A highly oblate nosetip (e.g., a flat nose or 5×1 ellipse), instead of a conventional spherical nose, was found to perform best under the considerations of aerodynamic stability, nosetip boundary-layer transition propagation, clear air shape change/recession, weather erosion resistance, re-entry vehicle re-entry range shortfall due to nose shape change, alleviation of frustum boundary-layer transition dispersion, and active nose transpiration cooled nosetip coolant requirements. Most of the advantages listed above are deduced from numerical results. More ground testing and flight experiments are needed to verify the analytical inference.

For the aft body, biconic geometries with $\theta_1 \approx 2\theta_2$ and $R_b \approx 2R_J$ are considered to be the optimum shape. Re-entry vehicles with these configurations would minimize the static margin movement with M_∞ and α. It would also decrease the effects of bluntness, which may exist during re-entry because of nose ablation. Recently, two sets of wind tunnel measurements suggested that the biconic joints have no perceptible influence on frustum boundary-layer transition behavior. Of course, the biggest advantage of bicone (or even tricone) is its potential flexibilities in meeting the ballistic coefficient requirements and booster sizing/warhead packaging.

The possible disadvantages for using the oblate nose as well as the biconic frustum in re-entry vehicle design have been discussed. The major uncertainties lie in its nosetip asymmetric ablation-induced trim and radar cross section electromagnetic performance. For instance, the high drag nosetip, e.g., flat-face nose, would probably result in a higher sheathing altitude as compared to that for a spherical nose.

References

[1] Miele, A., "Theory of Optimum Aerodynamic Shapes," *Applied Mathematics and Mechanics*, Vol. 9, Academic Press, New York, 1965, pp. 109-163.

[2] Aihara, Y., "Optimum Body Geometries of Minimum Heat Transfer at Hypersonic Speeds," *AIAA Journal*, Vol. 6, Nov. 1969, pp. 2187-2188.

[3] Hull, D. G., "On Hypersonic Shapes of Minimum Heat Transfer," *The Journal of the Astronautical Sciences*, Vol. XVII, No. 1, July-Aug. 1969, pp. 60-62.

[4] Perminov, V. D. and Solodkin, E. E., "Axisymmetric Bodies with Minimal Resistance and With Minimal Flow Toward the Surface of the Body, With Different Characters of the Flow in the Boundary Layer," Izvestiya Akademii Nauk SSSR, *Mekhanika Zhidkisti i Gaza*, Vol. 2, March-April 1971, pp. 94-102, English translation, Fluid Dynamics Consultant's Bureau, New York, 1973.

[5] Baker, R. L. and Kramer, R. F., "Reentry Vehicle Nosetip Design for Minimum Total Heat Transfer," AIAA Paper 79-201, New Orleans, La., Jan. 1979.

[6] Baker, R. L. and Kramer, R. F., "Nosetip Shape Optimization for Minimum Transpiration Coolant Requirements," *Progress in Aeronautics and Astronautics*, Vol. 59, *Aerodynamic Heating and Thermal Protection Systems*, edited by L.S. Fletcher, AIAA, New York, 1978, pp. 404-427.

[7] Yelmgren, K. E., "Optimum Nose Shape for Transpiration Cooled Reentry Vehicles," AFFDL TR-78-1117, Nov. 1978.

[8] Deborder, D. D. et al., "Stochastic Simulation of the Effects of Material Roughness Variability on Re-entry Vehicle Nosetip Transition Asymmetry and Trim Potential," GE Doc. 9160-FTS-TM-040, Nov. 1981; also, Breskman, D. G. et al., "Compilation and Correlation of GE223 Carbon Carbon Material Ablation Ground Test Data," SAMSO-TR-76-224, Oct. 30, 1976.

[9] Reda, D. C., "Comparative Transition Performance of Several Nosetip Materials as Defined by Ballistic Range Testings," *AIAA Journal*, Vol. 17, Nov. 1979, pp. 1201-1259.

[10] Kneen, K., "SSN-7 Nosetip Ablation Test Series in the AFWAL/AFFDL RENT 50 MW Arc Heater Facility," Acurex Tech. Rept. TR-81-15/AS, Acurex Corp., Mountain View, Calif., April 1981.

[11] Kessler, E., private communication, Aerojet Liquid Rocket Corp., Sacramento, Calif., 1981.

[12] Wilkinson, R., private communication TRW Systems Division, Redondo Beach, Calif., 1982.

[13] Dahm, T. J. et al., "Passive Nosetip Technology (PANT-II) Program, Vol. I, Inviscid Flow and Heat Transfer Modeling for Reentry Vehicle Nosetips," Acurex Corp., SAMSO-TR-77-11, Acurex Corp., Mountain View, Calif., Oct. 15, 1976.

[14] Uffelman, K. E. and Deffenbaugh, F. D., "Asymmetric Transition Effects on Reentry Vehicle Trim and Dispersion Characteristics," AIAA Paper 79-1626, Boulder, Colo., Aug. 1979.

[15] Auerbach, L., "Influence of Nosetip Shape on Boundary Layer Transition in Arc Heated Jets," AIAA Paper 78-235, Huntsville, Ala., Jan. 1978.

[16] Crose, J. G. et al., "Structure Technology for Advanced Reentry Systems," PDA Rept. 1041-00-09, Prototype Development Associates, Santa Ana, Calif., Aug. 1977.

[17] Hall, D. W. et al., "Alternate Configuration Investigations for Ballistic Reentry Vehicles," BMO-TR-81-76, Science Application Inc., Wayne, Pa., April 1980.

[18] Reinecki, W., "Shock Layer Shattering of Water Drops and Ice Crystals in Reentry Flight," AFML-TR-75-71, June 1975.

[19] Stetson, K. F. and Lewis, A. B., "Aerodynamic Comparison of a Conical and Biconic Reentry Vehicle," AIAA Paper 77-1161, Aug. 1977.

[20] Chaussee, D. S., Kutler, P., and Holtz, T., "Inviscid Supersonic/Hypersonic Body Flow Field and Aerodynamics from Shock-Capturing Technique Calculations," *Journal of Spacecraft*, Vol. 12, June 1976, pp. 325-331.

[21] Kochendorfer, P. C., "Aerodynamic Performance of a Range of Biconic Vehicle Configurations at Mach 10," PDA-TR-1353-64-43, Nov. 1979, Prototype Development Associates, Santa Ana, Calif.

[22] Smith, D. H. and Kochendorfer, P. C., "Boundary Layer Transition Tests on a Biconic Vehicle at Mach 9," BMO-TR-81-66, Prototype Development Associates, Santa Ana, Calif., Feb. 1981.

[23] Martellucci, A. and Makowski, F., "Performance Technology Program (PTP-S-II), Vol. V, Infrared Mapping Boundary Layer Transition on a Slender Cone," BMO-TR-81-2, Science Application Inc., Wayne, Pa., April 1970.

[24] Marvin J. G. and Sinclair, A. R., "Convective Heating in Regions of Large Favorable Pressure Gradient," *AIAA Journal*, Vol. 5, Nov. 1967, pp. 1940-1948.

[25] Inouye, M., Marvin, J. G., and Sinclair, A. R., "Comparison of Experimental and Theoretical Shock Shapes and Pressure Distributions on Flat-Faced Cylinder at Mach 10.5," NASA-TN-D-4397, Feb. 1968.

[26] Solomon, J. M., Ciment, M., Ferguson, R. E., and Bell, J. B., "Three-Dimensional Supersonic Inviscid Flow Field Calculations on Reentry Vehicle with Control Surfaces," AIAA Paper 77-84, Jan. 1977.

[27] Hall, D. W. and Dougherty, C. M., "Extension to the 3DSAP Approximate Inviscid Flow Field Code," BMO-TR-81-77, Science Application Inc., Wayne, Pa., Feb. 1981.